Integrated transition edge sensors on titanium in-diffused lithium niobate waveguides

Cite as: APL Photon. 4, 056103 (2019); doi: 10.1063/1.5086276
Submitted: 19 December 2018 • Accepted: 16 April 2019 •
Published Online: 7 May 2019

Jan Philipp Höpker,[1,a)] Thomas Gerrits,[2] Adriana Lita,[2] Stephan Krapick,[1] Harald Herrmann,[1] Raimund Ricken,[1] Viktor Quiring,[1] Richard Mirin,[2] Sae Woo Nam,[2] Christine Silberhorn,[1] and Tim J. Bartley[1]

AFFILIATIONS

[1] Department of Physics, Paderborn University, Warburger Str. 100, 33098 Paderborn, Germany
[2] National Institute of Standards and Technology, 325 Broadway, Boulder, Colorado 80305, USA

[a)] **Electronic mail:** jan.philipp.hoepker@upb.de

ABSTRACT

We show the proof-of-principle detection of light at 1550 nm coupled evanescently from a titanium in-diffused lithium niobate waveguide to a superconducting transition edge sensor. The coupling efficiency strongly depends on the polarization, the overlap between the evanescent field, and the detector structure. We experimentally demonstrate polarization sensitivity of this coupling as well as photon-number resolution of the integrated detector. The combination of transition edge sensors and lithium niobate waveguides can open the field for a variety of new quantum optics experiments.

I. INTRODUCTION

Integrated photonic circuits are widely used to realize compact and complex quantum optics experiments. They enable scalable creation and processing of quantum states which can be used in communication, computation, and simulation protocols to potentially outperform classical systems.[1] Lithium niobate is an established platform in the field of classical integrated optics because of its high second-order susceptibility and electro-optic properties.[2] Titanium in-diffused waveguides in lithium niobate are surface-guiding and offer low-loss waveguiding in both polarization directions (TE and TM), across a broad frequency range, making them ideal for a range of quantum optical circuits. For example, integrated single-photon sources using parametric down conversion[3,4] can be combined with electro-optic modulators[5,6] and active or passive routing to enable a variety of applications in quantum optics.[7] In addition, low-loss fiber pigtailing, by attaching single-mode fibers directly to the waveguide end-faces ("butt-coupling"), enables high overall system efficiency[3] and compatibility with the existing communication network infrastructure.

Until now, detection from lithium niobate waveguides has been restricted to fiber-coupled detectors, which adds an extra interface and associated losses. Of the various types of fiber-coupled detectors, those based on the breakdown of superconductivity offer the highest efficiency at telecom wavelengths and can be tailored for low timing-jitter, different photon numbers, or even photon-number resolution.[8–14] However, the positioning of fiber-coupled detectors with respect to an integrated optical circuit is limited, and their scaling towards complex circuitry is challenging.

Integrated detectors, using the coupling from an evanescent field of a waveguide into an on-chip detector, enable more complex circuitry, as they can be deposited at different positions inside the optical circuit. Furthermore, in an in-line geometry, nondetected (and nonscattered) photons remain inside the waveguide; this geometry potentially allows for further processing of undetected photons.[15] On platforms such as silicon or III-V semiconductor waveguides, the integration of superconducting nanowire single photon detectors (SNSPDs)[16–38] or transition edge sensors (TESs)[39,40] has been realized. However, the integration of single-photon detectors on lithium niobate waveguides is challenging.[41–43]

TESs operate at a transition stage between a superconductive and a normal resistance state.[44,45] When voltage-biased at their transition, the detector works as a microcalorimeter, which is sensitive to temperature changes introduced by single photon absorption even at infrared wavelengths. Using their weak electron-phonon coupling,

TESs made of thin-film tungsten have shown remarkable properties in terms of detection efficiency (95%–98%) and energy resolution (0.29 eV–0.42 eV).[12,13]

In this letter, we report on the first proof-of-principle evanescent single-photon detection with a transition edge sensor on a lithium niobate waveguide. This completes the toolbox for integrated quantum optics on this platform, adding integrated detection. We first show the waveguide fabrication and detector fabrication in Sec. II. In Sec. III, we describe simulations which estimate the detection efficiency. In Sec. IV, we show our experimental results including photon-number resolution up to six photons, system detection efficiency measurements for both polarizations, and first results for the energy resolution and decay time.

II. WAVEGUIDE AND DETECTOR FABRICATION

The waveguide fabrication starts with an 80 nm titanium deposition on a congruent lithium niobate wafer using e-beam evaporation, followed by a positive photoresist development. Under vacuum contact lithography and subsequent wet etching, 5 μm, 6 μm, and 7 μm wide titanium stripes are formed. These stripes are diffused into the lithium niobate substrate at 1060 °C, creating an index gradient from 2.211 to 2.214 in TE-polarization and 2.132 to 2.138 in TM-polarization at 1550 nm wavelength.[46–48] This way both polarizations (TE and TM) can be guided with losses below 0.1 dB/cm. A 2.5 cm long sample consisting of 70 waveguides is cut and its end-faces are polished. To ensure the waveguide quality, loss measurements are executed using an interferometric technique described by Regener and Sohler,[49] where similar loss values were achieved.

After ensuring the low-loss waveguiding, the TESs are deposited. Our integrated TES devices comprise a homogeneous 20 nm thick tungsten layer, deposited using magnetron sputtering. As 25 μm × 25 μm devices show high yield for fiber-coupled TESs, the same structure is chosen in this work. We placed three detectors per waveguide on top of a 2 nm amorphous silicon layer, which did not affect the optical properties of the detectors or waveguide, as ensured by further loss measurements, and additional niobium-contact pads for wire-bonding using photo lithography. A micrograph image of one device is shown in Fig. 1.

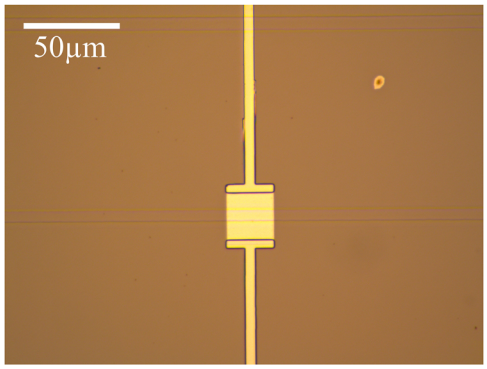

FIG. 1. Microscopic image of an integrated 25 μm × 25 μm × 20 nm tungsten TES on a 6 μm wide lithium niobate waveguide.

One benefit of titanium in-diffused waveguides on lithium niobate is the mode diameter which closely matches optical fiber. With this, a single-mode fiber ferrule can be directly glued to the polished waveguide end-face using a UV-sensitive adhesive. In this device, we used standard single-mode fiber (not polarization-maintaining), in order to simplify the pigtailing process. A precise, motorized alignment setup is used to ensure good coupling between the two interfaces. A thin layer of UV-glue with a fiber-matching refractive index is deposited in between the waveguide end-face and the fiber-ferrule and symmetrically cured using a ring of UV-LEDs for precuring and a UV-gun to fully harden the glue. To minimize displacement while cooling the pigtailed sample inside a cryostat,

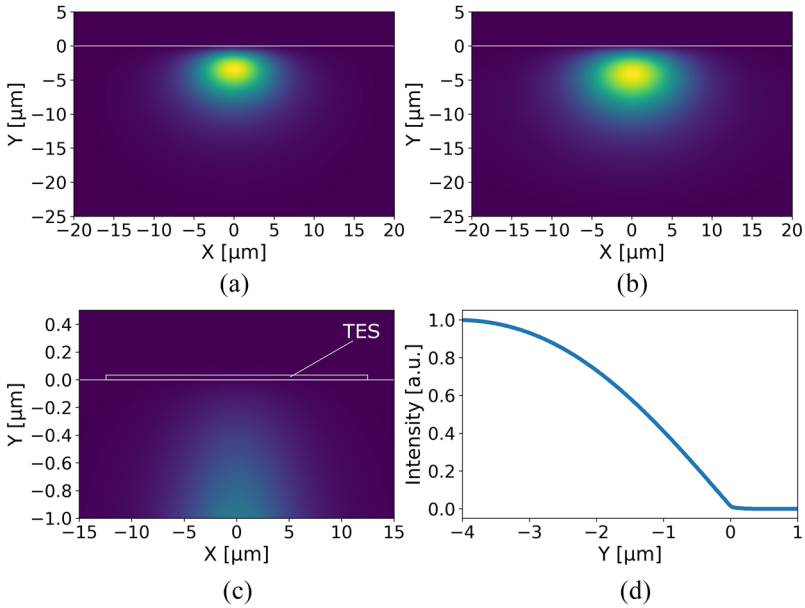

FIG. 2. Simulated polarization modes of a lithium niobate waveguide. (a) and (b) show the guided modes in TM-polarization and TE-polarization. (c) shows a close-up of the surface region for the TE-mode. In (d) the mode intensity of the TE-mode is plotted in the y-direction at X = 0 μm.

the thickness of the glue layer must be minimized and a symmetric spreading of the glue is preferable. At room-temperature, a theoretical maximum coupling to fiber of 92% can be achieved with the given mode overlap not including additional reflections between the glue and the sample which can be reduced by dielectric coatings.[3]

III. SIMULATIONS

As the guided modes inside the waveguide were optimized to match the mode diameter of a standard single-mode fiber, the overlap of the waveguide mode and the tungsten layer is very small. Therefore, the 25 μm × 25 μm × 20 nm device only sees a small part of the mode, as illustrated in Fig. 2. Finite-element-method and finite-difference beam propagation simulations were executed using a commercial mode-solver to estimate the detector efficiency for the given structure, using the refractive index of the waveguides based on Edwards,[46] Jundt,[47] and Strake[48] as well as independently measured values for the refractive index of tungsten. From these simulations a strong polarization dependence in the absorption was calculated, with values of 1.3% ± 0.6% in TM-polarization and 0.16% ± 0.06% in TE-polarization. Although the absorption, and therefore device efficiency, is small, modifications to the structure can be implemented to enhance the absorption as well as multiplexing several detetors.[40]

IV. RESULTS

We first tested the device under flood illumination, which showed successful electrical connection and optical response for the 25 μm × 25 μm × 20 nm devices.[42] Following this, the device was pigtailed and installed inside a dilution refrigerator (DR) to investigate the sensitivity of the evanescent field. The packaged device is robust and remains functional after several temperature cycles. The pigtailed fibers from the sample were spliced and connected from inside the DR to external FC/PC connectors and connected

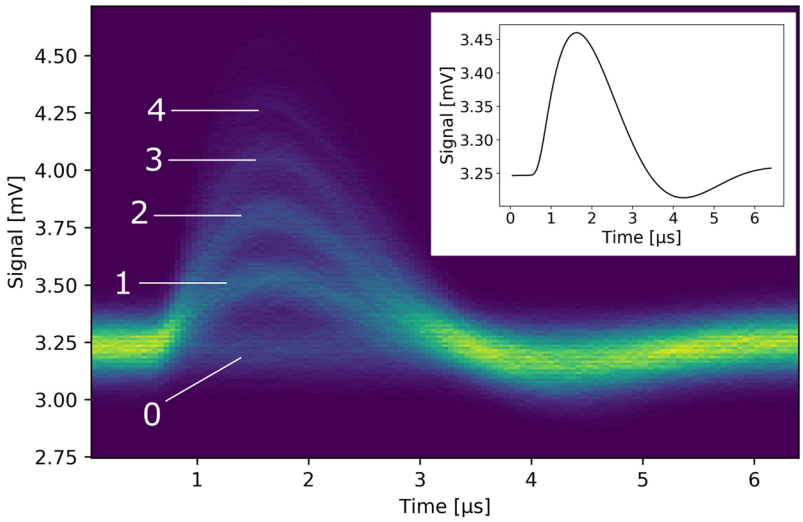

FIG. 3. Heatmap of measured photon traces with different peak heights corresponding to different photon numbers per pulse, pointed out by the displayed numbers, for an on-chip TES. The inset shows the average TES response.

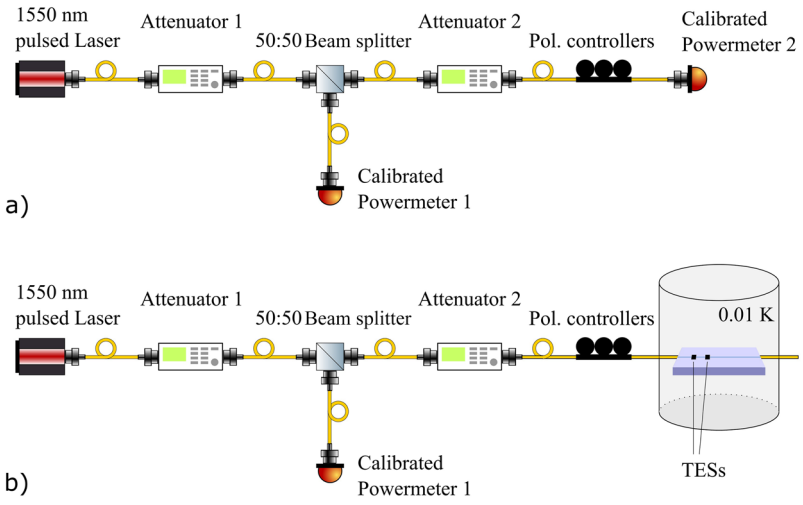

FIG. 4. Experimental scheme. The splitting ratio between the two arms is measured with two calibrated powermeters as shown in (a). In (b), the single-photon flux entering the cryostat is monitored.

to an attenuated pulsed 1550 nm laser with 50 ns laser pulses. As both end-faces of the waveguide were pigtailed, stable transmission through the waveguide at cold temperatures could also be verified. An overall transmission of 43% at room temperature and 8% ± 2% at 0.01 K was measured for both polarization directions. The lower transmission at room temperature compared to the predictions from simulations is caused by thicker glue layers and misalignment due to multiple pigtailing attempts. In addition, the waveguide end-faces are not coated, adding Fresnel reflections at the interfaces. The transmission drop at 0.01 K is due to an increased misalignment caused by the nonuniform glue layer undergoing thermal contraction. The polarization sensitivity of the mode overlap is negligible compared to the misalignment error. We observed approximately equal coupling at both sides of the waveguide chip. Therefore, assuming that both sides have nearly equal coupling, we estimated waveguide coupling efficiency (at each interface) of 66% at room temperature and 28% at 0.01 K. After optimizing the detector output, photon traces with different peak heights corresponding to different photon numbers per pulse could clearly be observed, as shown in Fig. 3.

The detector response for two detectors on the same waveguide was measured for different polarization settings and both coupling directions. We observed a strong polarization sensitivity but a small influence of the in-coupling direction, which verifies the evanescent coupling. When measuring scattered light, one would expect a large influence on the coupling direction, as the detectors are not symmetrically placed along the waveguide, as illustrated in Fig. 4(b).

From the measured photon traces of each detector and for each polarization setting, an average photon trace can be calculated as a template.[50] From the convolution of each trace and the template, every trace is converted into a single value proportional to peak height, from which we construct histograms for individual detectors, polarization setting, and in-coupling direction, as shown in Fig. 5. Also, an average (1/e) decay time of 1.6 μs can be calculated from the average photon trace. By using a Gaussian fit or by manually setting individual thresholds, the histogram can be compared to a Poisson distribution and therefore used to calculate a mean photon number. The detector efficiency equals the quotient of this calculated mean photon number and the expected mean photon number of the impinging photons. In addition, we can determine the energy resolution of the detectors from the histogram using the mean photon energy of the zero and one photon peak and its FWHM. We found an average energy resolution of 0.33 eV ± 0.05 eV, which is similar to other platforms. The timing and noise characteristics of the device, which were not optimized, were comparable with TES devices on other substrates. We observed a black-body count rate of 1000 cps and a rise-time jitter of 400 ns. Noise can be minimized by applying temporal filtering using the trace templates.

We measured the expected mean photon number using a splitting-ratio method, as illustrated in Fig. 4. In a first step, the splitting ratio between the two arms is investigated, using low attenuation on Attenuator 1 and high attenuation on Attenuator 2, which leads to high transmission at the calibrated Powermeter 1 and a lower but still measurable signal at the calibrated Powermeter 2. Next, Powermeter 2 is exchanged with a fiber that feeds into the cryostat and is pigtailed at the waveguide end-face. Using a high

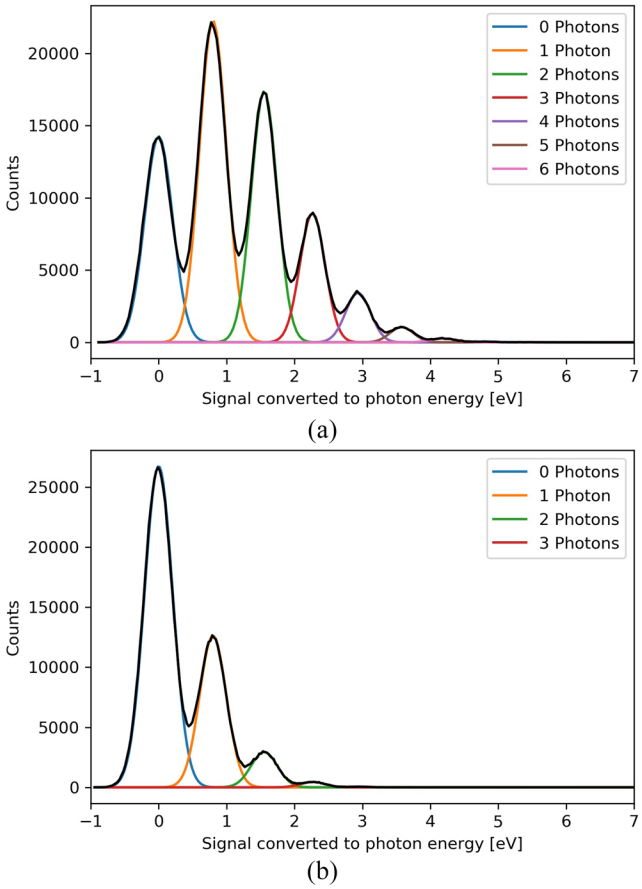

FIG. 5. Histograms of the evaluated photon traces converted to the underlying photon energies for one detector and Gaussian fitting for the individual peaks. (a) TM-polarization. (b) TE-polarization.

attenuation on Attenuator 1, while keeping Attenuator 2 fixed, reduces the output in both arms. Measuring the output at Powermeter 1 can be used to calculate the single-photon flux in the other arm.

From this, as well as an expected mean photon number, the maximum and minimum system detection efficiency (SDE) is calculated, depending on the polarization. This gives 0.23% ± 0.04% and 0.06% ± 0.01% for one detector and 0.19% ± 0.04% and 0.07% ± 0.01% for a second tested detector. The in-coupling direction has no influence on the SDE within the measurement accuracy.

The TES response was optimized by changing the polarization setting and monitoring the mean photon number using an *in situ* histogramming. From our room-temperature loss measurements and simulations, the maximum SDE was related to TM-polarization and the minimum SDE to TE-polarization. Further experiments using polarization maintaining fibers should be executed to verify this assumption. From transmission measurements through the pigtailed waveguide, we subtract coupling losses into the chip and calculate a corrected maximum detection efficiency of 0.8% per detector. Compared to simulations, the lower

efficiency can be attributed to a simplified model used to calculate the absorption in the simulations and to the polarization setting accuracy.

V. CONCLUSION

In this paper, we demonstrated the first proof-of-principle detection of single photons using TESs on lithium niobate waveguides. From the measured photon traces a histogram was calculated to confirm the photon-number resolution of the detectors. Light was coupled in from both directions into two detectors on the same waveguide and a strong polarization sensitivity was observed. Also, values for the average response decay time and energy resolution were calculated.

As an outlook, the detection efficiency can be significantly increased by changing the detector and/or waveguide geometry. As already shown on silica-on-silicon waveguides, additional tungsten fins (metallic absorptive strips deposited on the waveguide to conduct heat to the TES) can be used to increase the interaction length with the waveguide.[40] This can increase the evanescent coupling by at least one order of magnitude. Also tapering the lithium niobate waveguide and thereby increasing the mode confinement can increase the coupling efficiency. As a third option, additional dielectric layers can be used to manipulate the waveguide mode and pull it closer to the waveguide surface, also resulting in better coupling to the detector, as shown in the simulation results in Fig. 6. Here, the cover refractive index was changed using different nonabsorbing materials (SiO_2, ZnO, and Ta_2O_5), which results in the center of the mode being pulled closer to the detector and therefore higher absorption. The detector lengths considered are in line with previously demonstrated geometries.[40,42]

Furthermore, the system detection efficiency can be enhanced by detector multiplexing. However, it is not yet apparent, if it is possible to outperform end-face coupled TESs with on-chip detectors on lithium niobate when improving the evanescent coupling, but very promising when upscaling the number of detectors per chip.

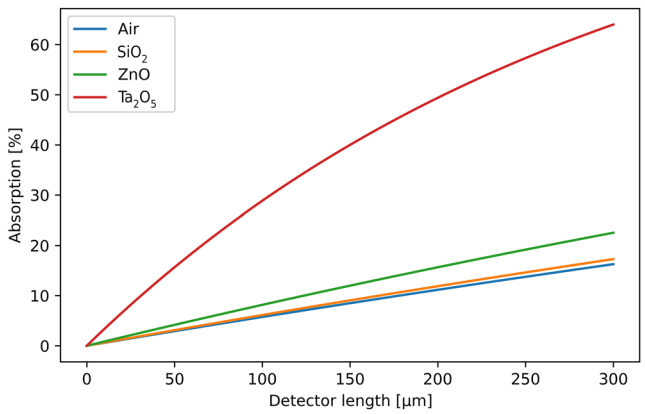

FIG. 6. Simulated detector absorption over detector length for a 4 μm wide and 20 nm high tungsten fin on top of a waveguide[40,42] for 1550 nm TM-polarized light with different nonabsorbing materials as a widespread cover layer.

ACKNOWLEDGMENTS

The study was funded by the Deutsche Forschungsgemeinschaft (DFG, German Research Foundation)—Projektnummer No. 231447078—TRR 142. This is a contribution of NIST, an agency of the U.S. government, not subject to copyright.

REFERENCES

[1] I. A. Walmsley, "Quantum optics: Science and technology in a new light," Science **348**(6234), 525–530 (2015).
[2] W. Sohler *et al.*, "Integrated optical devices in lithium niobate," Opt. Photonics News **19**(1), 24–31 (2008).
[3] N. Montaut *et al.*, "High-efficiency plug-and-play source of heralded single photons," Phys. Rev. Appl. **8**, 024021 (2017).
[4] S. Krapick *et al.*, "An efficient integrated two-color source for heralded single photons," New J. Phys. **15**, 033010 (2013).
[5] N. Moeini *et al.*, "Electro-optic polarization controller with Ti:PPLN channel waveguides," in Proceedings of European Conference on Integrated Optics (ECIO), 2010.
[6] C. Y. Huang *et al.*, "Electro-optic Ti:PPLN waveguide as efficient optical wavelength filter and polarization mode converter," Opt. Express **15**(5), 2548–2554 (2007).
[7] P. R. Sharapova *et al.*, "Toolbox for the design of $LiNbO_3$-based passive and active integrated quantum circuits," New J. Phys. **19**, 123009 (2017).
[8] A. Migdall *et al.*, *Single-Photon Generation and Detection* (Academic Press, 2013), Vol. 45.
[9] R. H. Hadfield and G. Johansson, *Superconducting Devices in Quantum Optics* (Springer, 2016).
[10] C. M. Natarajan *et al.*, "Superconducting nanowire single-photon detectors: Physics and applications," Supercond. Sci. Technol. **25**, 063001 (2012).
[11] F. Marsili *et al.*, "Detecting single infrared photons with 93% system efficiency," Nat. Photonics **7**, 210–214 (2013).
[12] A. Lita *et al.*, "Counting near-infrared single-photons with 95% efficiency," Opt. Express **16**(5), 3032–3040 (2008).
[13] D. Fukuda *et al.*, "Titanium-based transition-edge photon number resolving detector with 98% detection efficiency with index-matched small-gap fiber coupling," Opt. Express **19**(2), 870–875 (2011).
[14] T. Gerrits *et al.*, "Extending single-photon optimized superconducting transition edge sensors beyond the single-photon counting regime," Opt. Express **20**(21), 23798–23810 (2012).
[15] X. Hu *et al.*, "Efficiently coupling light to superconducting nanowire single-photon detectors," IEEE Trans. Appl. Supercond. **19**(3), 336–340 (2009).
[16] J. P. Sprengers, "Waveguide superconducting single-photon detectors for integrated quantum photonic circuits," Appl. Phys. Lett. **99**, 181110 (2011).
[17] S. Jahanmirinejad *et al.*, "Photon-number resolving detector based on a series array of superconducting nanowires," Appl. Phys. Lett. **101**, 072602 (2012).
[18] G. Reithmaier *et al.*, "On-chip time resolved detection of quantum dot emission using integrated superconducting single photon detectors," Sci. Rep. **3**, 1901 (2013).
[19] D. Sahin *et al.*, "Waveguide photon-number-resolving detectors for quantum photonic integrated circuits," Appl. Phys. Lett. **103**, 111116 (2013).
[20] Z. Zhou *et al.*, "Superconducting series nanowire detector counting up to twelve photons," Opt. Express **22**(3), 3475–3489 (2014).
[21] M. Kaniber *et al.*, "Integrated superconducting detectors on semiconductors for quantum optics applications," Appl. Phys. B **122**, 115 (2016).
[22] F. Najafi *et al.*, "On-chip detection of non-classical light by scalable integration of single-photon detectors," Nat. Commun. **6**, 6873 (2015).
[23] F. Mattioli *et al.*, "Photon-counting and analog operation of a 24-pixel photon number resolving detector based on superconducting nanowires," Opt. Express **24**(8), 9067–9076 (2016).

[24]J. Li *et al.*, "Nano-optical single-photon response mapping of waveguide integrated molybdenum silicide (MoSi) superconducting nanowires," Opt. Express **24**(13), 13931–13938 (2016).
[25]W. H. P. Pernice *et al.*, "High-speed and high-efficiency travelling wave single-photon detectors embedded in nanophotonic circuits," Nat. Commun. **3**, 1325 (2012).
[26]M. K. Akhlaghi *et al.*, "Waveguide integrated superconducting single-photon detectors implemented as near-perfect absorbers of coherent radiation," Nat. Commun. **6**, 8233 (2015).
[27]P. Cavalier *et al.*, "Light interference detection on-chip by integrated SNSPD counters," AIP Adv. **1**, 042120 (2011).
[28]S. Ferrari *et al.*, "Waveguide-integrated single- and multi-photon detection at telecom wavelengths using superconducting nanowires," Appl. Phys. Lett. **106**, 151101 (2015).
[29]O. Kahl *et al.*, "Waveguide integrated superconducting single-photon detectors with high internal quantum efficiency at telecom wavelengths," Sci. Rep. **5**, 10941 (2015).
[30]C. Schuck *et al.*, "NbTiN superconducting nanowire detectors for visible and telecom wavelengths single photon counting on Si_3N_4 photonic circuits," Appl. Phys. Lett. **102**, 051101 (2013).
[31]C. Schuck *et al.*, "Waveguide integrated low noise NbTiN nanowire single-photon detectors with milli-Hz dark count rate," Sci. Rep. **3**, 1893 (2013).
[32]C. Schuck *et al.*, "Quantum interference in heterogeneous superconducting-photonic circuits on a silicon chip," Nat. Commun. **7**, 10352 (2016).
[33]A. Beyer *et al.*, "Waveguide-coupled superconducting nanowire single-photon detectors," in *Conference on Lasers and Electro-Optics (CLEO)* (Optical Society of America, 2015), pp. 1–2.
[34]J. M. Shainline *et al.*, "Room-temperature-deposited dielectrics and superconductors for integrated photonics," Opt. Express **25**(9), 10322–10334 (2017).
[35]P. Rath *et al.*, "Superconducting single-photon detectors integrated with diamond nanophotonic circuits," Light: Sci. Appl. **4**, e338 (2015).
[36]H. A. Atikian *et al.*, "Superconducting nanowire single photon detector on diamond," Appl. Phys. Lett. **104**, 122602 (2014).
[37]R. W. Heeres *et al.*, "On-chip single plasmon detection," Nano Lett. **10**(2), 661–664 (2010).
[38]R. W. Heeres *et al.*, "Quantum interference in plasmonic circuits," Nat. Nanotechnol. **8**, 719–722 (2013).
[39]T. Gerrits *et al.*, "On-chip, photon-number-resolving, telecommunication-band detectors for scalable photonic information processing," Phys. Rev. A **84**, 060301 (2011).
[40]B. Calkins *et al.*, "High quantum-efficiency photon-number-resolving detector for photonic on-chip information processing," Opt. Express **21**(19), 22657–22670 (2013).
[41]M. G. Tanner *et al.*, "A superconducting nanowire single photon detector on lithium niobate," Nanotechnology **23**, 505201 (2012).
[42]J. P. Hoepker *et al.*, "Towards integrated superconducting detectors on lithium niobate waveguides," Proc. SPIE **10358**, 1035809 (2017).
[43]E. Smirnov *et al.*, "Superconducting nanowire single-photon detector on lithium niobate," J. Phys.: Conf. Ser. **1124**, 051025 (2018).
[44]B. Cabrera *et al.*, "Detection of single infrared, optical, and ultraviolet photons using superconducting transition edge sensors," Appl. Phys. Lett. **73**(6), 735–737 (1998).
[45]A. J. Miller *et al.*, "Demonstration of a low-noise near-infrared photon counter with multiphoton discrimination," Appl. Phys. Lett. **83**(4), 791–793 (2003).
[46]G. J. Edwards and M. Lawrence, "A temperature-dependent dispersion equation for congruently grown lithium niobate," Opt. Quantum Electron. **16**, 373–375 (1984).
[47]D. H. Jundt, "Temperature-dependent Sellmeier equation for the index or refraction, ne, in congruent lithium niobate," Opt. Lett. **22**(20), 1553–1555 (1997).
[48]E. Strake *et al.*, "Guide modes of Ti:$LiNbO_3$ channel waveguides: A novel quasi-analytical technique in comparison with the scalar finite-element method," J. Lightwave Technol. **6**(6), 1126–1135 (1988).
[49]R. Regener and W. Sohler, "Loss in low-finesse Ti:$LiNbO_3$ optical waveguide resonators," Appl. Phys. B **36**, 143–147 (1984).
[50]D. J. Fixsen *et al.*, "Optimal energy measurement in nonlinear systems: An application of differential geometry," J. Low Temp. Phys. **176**(1-2), 16–26 (2014).